10.21611/qirt.2023.13

Diagnostic Tool for Diabetic Retinopathy using Thermal Eye Images

Nithya Rajagopalan*, K. Nirmala*, M. Vahini*, S. Nisha* and S. Rakshitha*

*Sri Sivsubramaniya Nadar College of Engineering, Chennai, Tamil Nadu, India, nithyar@ssn.edu.in

ABSTRACT:

Diabetic Retinopathy (DR) occurs as an effect of Diabetes, affecting the retina causing loss of vision. Worldwide 27% of the diabetic individuals are estimated to have DR, leading to 0.4 million blindness. As the DR population increases every year, early diagnosis is the need of the hour to avoid further progression of the disease thereby preventing blindness. In this work, DR diagnosis is performed using thermal images of the eye. According to earlier research on the eye, the increase in ocular surface temperature caused by dilatation is less in individuals with diabetic retinopathy than in control participants, making it a possible parameter for DR diagnosis. This imaging modality is non-invasive and less time consuming making it an easier diagnostic tool for large scale screening. For this work real time images are acquired from both the eyes of 20 DR participants and 16 control participants, with a total of 62 thermal eye images. The significant features from the pre-processed thermal eye images are extracted using Scale invariant transform and Gabor Transform methods. The extracted features are processed using optimal Machine learning algorithms to classify DR images from normal images. The diagnostic accuracy of the proposed tools is 96%. The results indicate that the IR thermal imaging system could be an efficient method for the non-invasive and non-contact detection of thermal anomalies in the eyes of patients with diabetes.

Keywords: Diabetic Retinopathy, Infrared Thermal Imaging, Scale invariant transform, convolution neural networks

1. Introduction

The human eye frequently exhibits manifestations of common diseases, with diabetic retinopathy, age-related macular degeneration, glaucoma, and cardiovascular disease being the most prevalent among them [1,2]. Diabetic Retinopathy (DR) is common in diabetic individuals with an incidence of up to 34.6 % globally [3]. DR, in its early stages, begins with parts of the retina being considerably higher in temperature than the rest of the eye. Blood flow will be disturbed and causes swollen, leaking, damaged blood vessels resulting in fuzzy vision. Early detection of diabetic retinopathy is crucial because it allows for timely intervention and treatment, which can help prevent the condition from advancing to more severe stages. Without any treatment, diabetic retinopathy can lead to irreparable impairment and eventual blindness [4]. However, manually detecting retinal changes is a challenging and time-consuming process. Therefore, the creation of a system with the ability to automatically assess the retina and monitor the disease's progression would be immensely beneficial for both patients and ophthalmologists.

According to the worldwide clinical diabetic retinopathy disease severity scale the existence of diabetic retinopathy can be divided into five categories as None, Mild, Moderate, Severe, and Proliferative. Microaneurysms are also a defining feature of mild DR. The diameter of microaneurysms is typically between 10 and 100 m, which is smaller than the diameter of the major veins in the eye. Moderate diabetic retinopathy (DR) represents an intermediary stage that falls between mild and severe retinopathy [5,6]. The extreme case of DR is proliferative retinopathy. When the cells in the back of the eye receive insufficient oxygen, new blood vessels begin to form. They are brittle, and bleeding could result in a blood clot. Retina can become dislodged and cause irreversible eyesight loss [6].

Patients suffering from diabetic retinopathy reported a decline in ocular blood flow (OBF), and this decrease is found to be associated with the advancement of the disease. Ocular blood flow decline was seen in patients with diabetic retinopathy and was associated with the disease's progression [7]. Ocular surface temperature (OST) is a metric based on ambient temperature, body temperature, and infrared thermography-measured ocular blood flow. Sodi et. Al [8] analyzed a group of DR and healthy patients and observed a notable distinction between the two groups, with diabetic eyes displaying lower values of OST.

Thermal Imaging is gaining recognition in the medical field, especially post-pandemic times [9,10], its applications ranging from fever screening to non-invasive tumour detection. Infrared (IR) thermography represents a temperature measurement method that doesn't require physical contact or intrusion, making it capable of presenting the current distribution of surface temperatures in real-time [11]. Thermography serves as an investigative method enabling the swift and visual representation of temperature variation across a broad surface through the utilization of infrared sensing, often displayed with a color-coded system [12]. It is even considered passive, as it doesn't involve the emission of potentially harmful radiation through the biological system; instead, it solely captures the natural body heat emitted by the subject. In the realm of medicine, thermography has been extensively employed for diagnosing conditions like breast cancer,

diabetes-related diseases, dentistry, as well as various eye conditions such as glaucoma and dry eyes, among others [13]. A highly innovative application of thermal imaging in the medical domain would be to detect the DR in its preliminary stages. The overall change in the temperature of the eye region can be an important contributing factor in diagnosing DR.

Previous research on the eye has indicated that the increase in ocular surface temperature due to dilation is less pronounced in individuals with diabetic retinopathy compared to control participants serving as a diagnostic parameter for diabetic retinopathy [14]. The expansion of the pupil revealed a rise in OST among both control subjects and individuals with diabetic retinopathy. However, the extent of this increase was notably lower when compared to the control group. It was concluded by Chandrasekar B et al [15] that the fluctuation in OST seen in patients with diabetic retinopathy during pre- and post-dilation experiments is an indication of pathology and can be employed as a diagnostic measure.

2. Methodology

The step-by-step process proposed for detecting Diabetic Retinopathy in ocular thermal images is shown in detail in Figure 1. At first, protocols for capturing ocular thermal images were devised, thus generating a database containing images from both healthy individuals (the control group) and Diabetic Retinopathy participants. Subsequently, the images undergo pre-processing, which includes resizing and cropping to isolate the region of interest. Image augmentation is then applied to enhance data diversity and quantity for training. Following this, feature extraction is performed, and the extracted features are fed into optimized Machine Learning algorithms for classification.

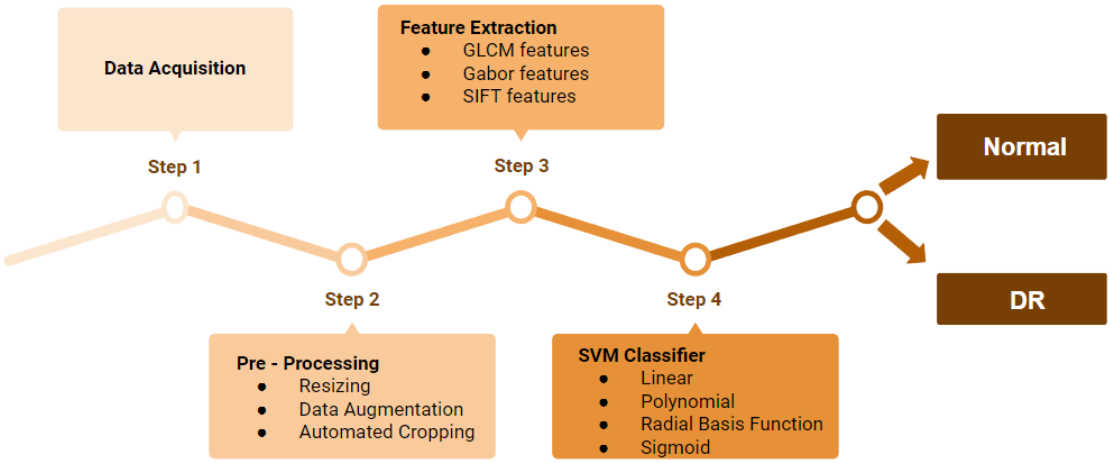

Fig. 1. *Methodology*

2.1. Data Acquisition

The current study analysed the ocular IR images of the patients regardless of any ailments using Forward-looking infrared (FLIR) camera with 161,472-pixel resolution (464 x 348) resolution. Participants were briefed about the experimental procedure of thermal image acquisition, and written approval was procured from each participant before the study commenced. The camera was affixed to a tripod easel, maintaining a fixed gap of 50cm between the camera and the subjects, and the ambient temperature was controlled at 20℃. Prior to screening, the camera was calibrated to ensure accuracy and stability. To prevent outside infrared radiation from entering the room, all windows were covered or shielded, and the room temperature was maintained between 18℃ and 23℃. All of the volunteers for the control group self-identified as being in good health, not smokers, fairly active, and free of any previous cases of retinopathy, diabetes, or hypertension.

A total of 72 images from both the eyes of 20 DR participants and 16 control participants were acquired. According to infrared thermography (IR), the data show a thermal change in the surface temperature as shown in Figure 2.

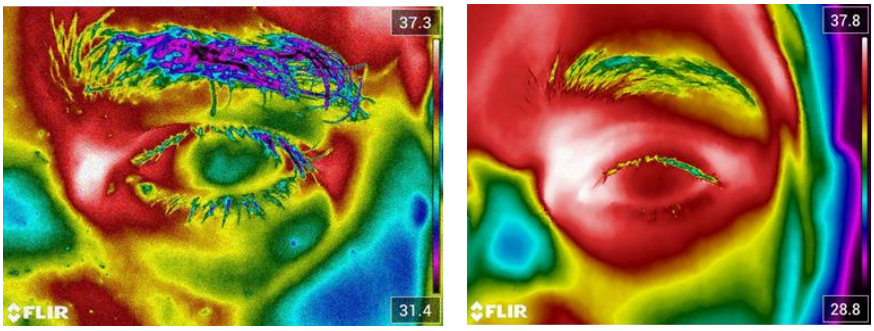

(a) ***(b)***

Fig. 2. *Thermal image of (a) DR eye (b) Normal eye*

Colour is a potent descriptor in IR images, and it is used to describe temperature variations [16,17]. Typically, hotter and colder regions are depicted in red and blue, respectively, with yellow and green representing the temperature differences between these extremes. A notable difference between the two groups was identified, as illustrated in Figure 2, wherein the ocular surface temperature (OST) values were consistently lower in the eyes affected by diabetic retinopathy, represented by the green coloration. Within the cohort of examined DR eyes, a distinct thermographic pattern emerged, characterized by elevated temperatures at the peripheries and correspondingly lower temperatures at the central region which aligns with prior findings of thermographic profiles of ocular surface temperature. In contrast, the normal eyes exhibited a comparatively uniform high temperature, with only minimal temperature fluctuations observed at both the extremes and the centre denoted by the red coloration.

2.2 Image Pre – Processing

The images were initially resized to 500x500 before undergoing cropping to ensure that the machine learning model is fed with input images of uniform dimensions as shown in Figure 3. The original dimension of all the images in the dataset is 640x480 pixels, which makes processing them time-consuming [18]. To ease such execution complexities and prevent overfitting, resizing is performed.

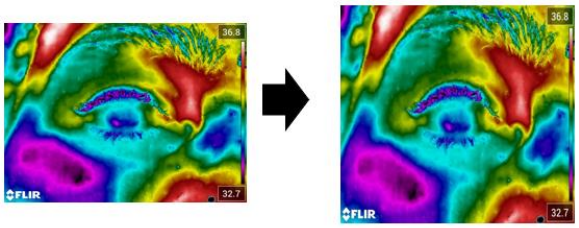

Original size 640x480 **Resized image 500x500**

Fig. 3. *Image Resizing*

Image augmentation techniques were accomplished to the acquired dataset to artificially expand the dataset in order to enhance the diversity and amount of training data. The augmented image data-set helps in a more efficient model training process with more data and accuracy [19,20]. Spatial augmentation techniques include – Flipping, Rotation, Shifting, Random noise and Gaussian blur were used. Specifically, the DR dataset was augmented to 800 images, while the normal images underwent augmentation to a total of 850 images.

The images were flipped vertically and horizontally. Rotating generates clockwise or counterclockwise rotated images by the provided angle - 45^{O},90^{O} and 180^{O}, repositioning objects in the image. A positive angle rotates an image in an anticlockwise direction, while a negative angle rotates the image in a clockwise direction. In this study, the images have been shifted vertically by 40 units in pixels to ensure that the region of interest is not lost.

Gaussian noise is added to the images which is useful for regularisation and reduces overfitting. Gaussian noise is statistical noise with a zero mean normal distribution probability density function and standard deviation value. The standard deviation value was given as 180 which determines the intensity of the noise. Gaussian blur is added to the images that takes an image and kernel size as the parameters. The kernel size determines the degree of blur added to the image. As a result, an 11x11 pixel kernel size Gaussian blur is used. Therefore, a kernel size of 11x11 pixels produces a medium level of blur. Haar cascade method was employed that used the coordinates of the eyes to crop off the region

of interest in an effort to automate the cropping procedure for the acquired image dataset. It required precise parameter settings to effectively detect eyes in the images. However, other methods such as histogram of oriented gradients and canny edge detection algorithm resulted in a significant number of incorrect detections, rendering the technique ineffective.

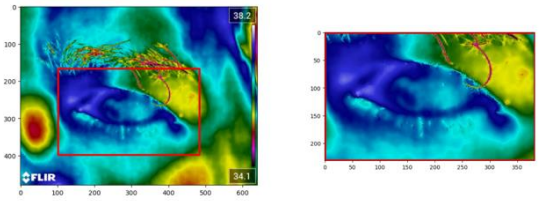

Fig. 4. *Automated Cropping using haar cascade algorithm*

2.3. Feature Extraction

Feature extraction entails separating the visual details from an image and converting it into feature vectors that are stored in a specific feature database. The augmented images mentioned in the previous step are used to extract features in this study. The techniques used to extract the features include GLCM, SIFT, Gabor.

2.3.1. Extraction of GLCM Features

The Gray level Co-occurrence Matrix (GLCM) calculates how often a pixel with gray-level value 'i' appears next to an adjacent pixel with the value "j" in a horizontal, vertical, or diagonal direction [21]. Thermal images are used to capture and display variations in temperature. GLCM helps capture and quantify these temperature patterns as texture features, making it easier to detect anomalies or irregularities in the IR data. Texture characteristics are determined by analysing the statistical distribution of observed intensity combinations at predefined positions in relation to one another within the image [22]. The second order GLCM statistical texture features on thermal images are obtained and following features are taken into consideration: Contrast, Energy, Correlation, Homogeneity. Contrast provides an assessment of the intensity contrast between a pixel and its neighbouring pixels across the entire image. Energy quantifies the sum of squared elements within the GLCM. Correlation offers an indication of the level of correlation between a pixel and its neighbouring pixels throughout the entire image. Homogeneity furnishes a metric for measuring the proximity of the element distribution within the GLCM to its diagonal.

$$Energy = \sum_{i=0}^{L-1}\sum_{j=0}^{L-1} p^2(i,j) \qquad (1)$$

$$Local\ Homogeneity = \sum_{i=0}^{L-1}\sum_{j=0}^{L-1} \frac{p(i,j)}{1+|i-j|} \qquad (2)$$

$$Contrast = \frac{1}{(L-1)^2} \quad \sum_{i=0}^{L-1}\sum_{j=0}^{L-1}(i-j)^2 p(i,j) \qquad (3)$$

$$Correlation = \frac{\sum_{i=0}^{L-1}\sum_{j=0}^{L-1}(i\times j)p(i,j) - \mu_h\mu_v}{\sigma_h\sigma_v} \qquad (4)$$

where p(i,j) represents input image, L denotes the overall amount of utilised grey levels μh & μv = Mean, h & σv = Standard deviation for the elements of co-occurrence matrices in the horizontal and vertical directions.

2.3.2. Extraction of SIFT features

SIFT (Scale-Invariant Feature Transform) is used to extract local features that remain invariant to variations in scale, rotation, and illumination in images. SIFT operates by detecting and characterizing keypoints within an image. These keypoints are chosen for their unique and stable appearance across different scales and orientations. Once identified, SIFT computes a feature vector for each keypoint, encapsulating its distinctive visual information. These feature vectors are not only highly discriminative but also resistant to common image transformations, rendering them indispensable for tasks that demand robust and accurate feature extraction [24].

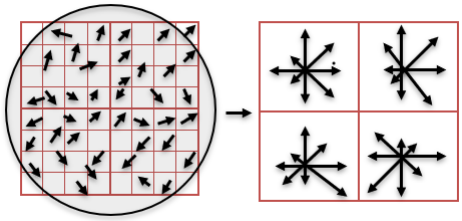

***Fig. 5**. Keypoint Descriptors*

SIFT in Thermal Image Feature Extraction: Thermal images present a unique set of challenges in feature extraction due to their distinct characteristics, including variations in thermal radiation intensity and subtle temperature differences. SIFT proves to be an invaluable asset in this context. Its ability to capture and describe distinctive local features, regardless of thermal variations, equips it with the capacity to identify critical patterns within thermal images.

The concept of scale space involves applying a range of Gaussian filters with varying values for the sigma parameter to the target image. The resulting plot is referred to as the Scale Space [25]. In choosing the Scale Space Peaks, the Spatial Coincidence Assumption plays a crucial role. This assumption means that an edge is considered a genuine edge if it is identified at the same position across different scales, represented by zero crossings in the scale space. The first step in the process involves computing the scale space selection and keypoint localization. The process of key point localization includes improving the key points that were chosen in the earlier step. Keypoints with low contrast, those that are shaky, and those that are perched on edges are removed. The values of the extrema are determined by computing the Laplacian of key points identified in the earlier stage as shown in Eq. 5.

$$Z = -\frac{\partial^2 D^{-1}}{\partial x^2}\frac{\partial D}{\partial x} \qquad (5)$$

***Eq. 5.** DoG for keypoints*

The keypoint descriptor is created by expressing the 128 bin values as a vector. This vector is then normalised to unit length to make it invariant to scale and rotation changes. The resulting descriptor is robust to changes in lighting, contrast, and viewpoint.

Utilizing k-means Clustering for SIFT in Thermal Image Analysis:

In the presented application, the power of SIFT for feature extraction in thermal images is harnessed. To further enhance its efficacy, k-means clustering is employed. SIFT descriptors and image patches are extracted at SIFT keypoint positions. The targets and related patches are represented as input for the SVM classifier, which operates on the cluster indices derived from the clustered SIFT descriptors [26]. Figure 6 explains the methodology involved in partitioning the SIFT descriptors into clusters, using k-means with a predetermined number of clusters, in our case, 100. This process effectively grouped similar SIFT descriptors, creating a compact representation of the image's visual content. The resulting clusters served as a visual dictionary, enabling us to succinctly describe the distinctive patterns and structures within thermal images.

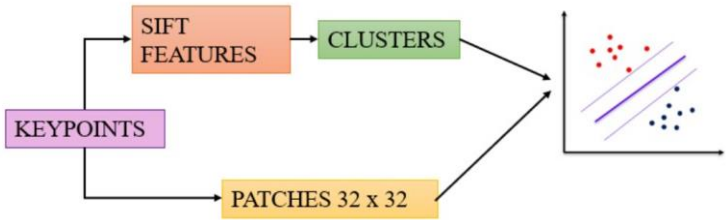

***Fig. 6.** Overview of the unsupervised feature learning.*

Thus, SIFT stands as a pivotal technique in the domain of image analysis, offering unmatched robustness in capturing distinctive features across various applications. In the context of thermal images, SIFT emerges as a potent tool, capable of extracting valuable information even in the presence of thermal variations. Our utilization of k-means clustering underscores the versatility of this method, promising advancements in the field of thermal image analysis and offering new opportunities for enhanced pattern recognition and understanding in the realm of thermal imaging.

2.3.3. Extraction of Gabor Features

Gabor filters are used to extract the textural micropatterns in an image like lines, edges and spots [27]. Gabor filters can be adjusted with various orientations and scales to extract spatial textural features in regions of interest, which could be highly helpful for detecting diabetic retinopathy. The Gabor transform combines a Gaussian window and a short-term Fourier transformation in order to analyse data in the spatial domain. The 2D Gabor filter is a powerful sinusoidally modulated Gaussian function with a spatial response [28]. The sinusoidal input determines the direction of the filter, while the weights are supplied by the Gaussian wave. The Gabor filter can detect edges and extract features from images with high accuracy of certain frequency and orientation by fusing these two factors together [29]. The 2D Gabor filter has two components, a real part and an imaginary part, that represent orthogonal directions. These two components can be combined into a complex number, or used separately to analyse different aspects in an image, Eq. 6.

$$\text{Complex:} \quad g(x,y;\lambda,\theta,\varphi,\sigma,\gamma) = exp\left(-\frac{x^2+\gamma^2y^2}{2\sigma^2}\right) exp\left(i\left(2\pi\frac{x}{\lambda}+\varphi\right)\right) \tag{6}$$

The parameter λ determines the width of the strips in the Gabor function. Meanwhile, Θ dictates the orientation of the Gaussian envelope, ranging from 0 to π. As for ɣ, it represents the aspect ratio, which controls the height of the Gabor function. When ɣ is set to 0 (a high aspect ratio), the filter resembles a vertical slit (with Θ at 90 degrees), while values close to 1 result in a nearly spherical kernel, resembling a Gaussian filter. The σ parameter is responsible for defining the spread of the Gaussian function. If a large σ is applied to small features, it may miss those features entirely, resulting in lower spatial resolution, and vice versa. Lastly, the parameter Ψ influences the symmetry of the Gabor filter [30,31].

To obtain texture features from an image, a bank of 2D Gabor filters are generated with variable parameters such as orientation and aspect ratio. In Figure 7, a 2D Gabor kernel is shown with different rotation angles.

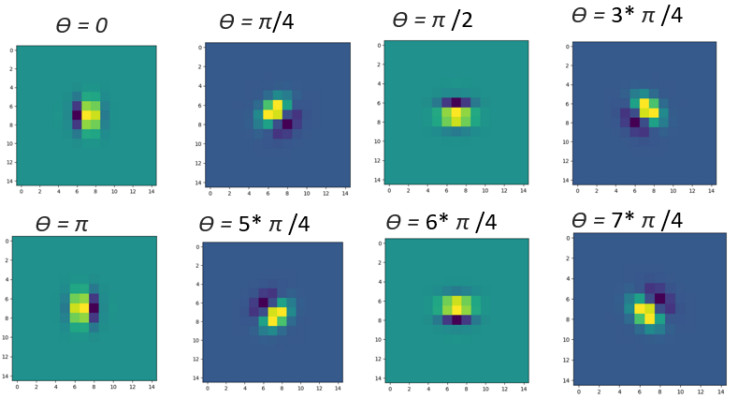

Fig. 7. *A 2D Gabor bank with different Θ values*

In the thermal eye dataset, specific parameter values are chosen to optimize the Gabor filtering process. These parameters include setting the gamma values to 0.9 and 1 in order to obtain spherical kernels, which are effective for detecting the region of interest (eyeball). Additionally, the sigma values are set to 0.5 and 1, as using large sigma values on small features may cause important features to be missed. These Gabor filters are convolved with the input images, resulting in Gabor filtered images. Statistical features are derived from the images that have undergone Gabor filtering. Specifically, statistical moments are computed to depict the characteristics of the coefficient distribution function. These statistical moments encompass the first four orders: mean (μ) defines the average value of the distribution, variance (σ^2) describes the measure of the spread of the distribution, skewness (γ) quantifies the distribution's asymmetry and kurtosis (β) gives information about the peakedness of the distribution. These moments provide insight into the characteristics of the coefficient distribution derived from the Gabor filtered images that serve as concise descriptors of the distribution of

Gabor filter coefficients, providing information about the texture and features present in the images. If P is the input image, then the first four orders of statistical features are computed by Equations (7) to (10).

$$\text{Mean } (\mu) = E[P] \tag{7}$$

$$\text{Variance } (\sigma^2) = E\left[(P - \mu)^2\right] \tag{8}$$

$$\text{Skewness } (\gamma) = E\left[\left(\frac{P-\mu}{\sigma}\right)^3\right] \tag{9}$$

$$\text{Kurtosis } (\beta) = \frac{E\left[(P-\mu)^4\right]}{\left(E\left[(P-\mu)^2\right]\right)^2} \tag{10}$$

The aforementioned features are computed for a specific input image along with a set of Gabor kernels. This process systematically goes through different combinations of parameters to generate Gabor kernels. Consequently, each input image is convolved with these distinct Gabor kernels. As a result, for a single image, a total of 32 unique filtered images are produced as shown in Figure 8.

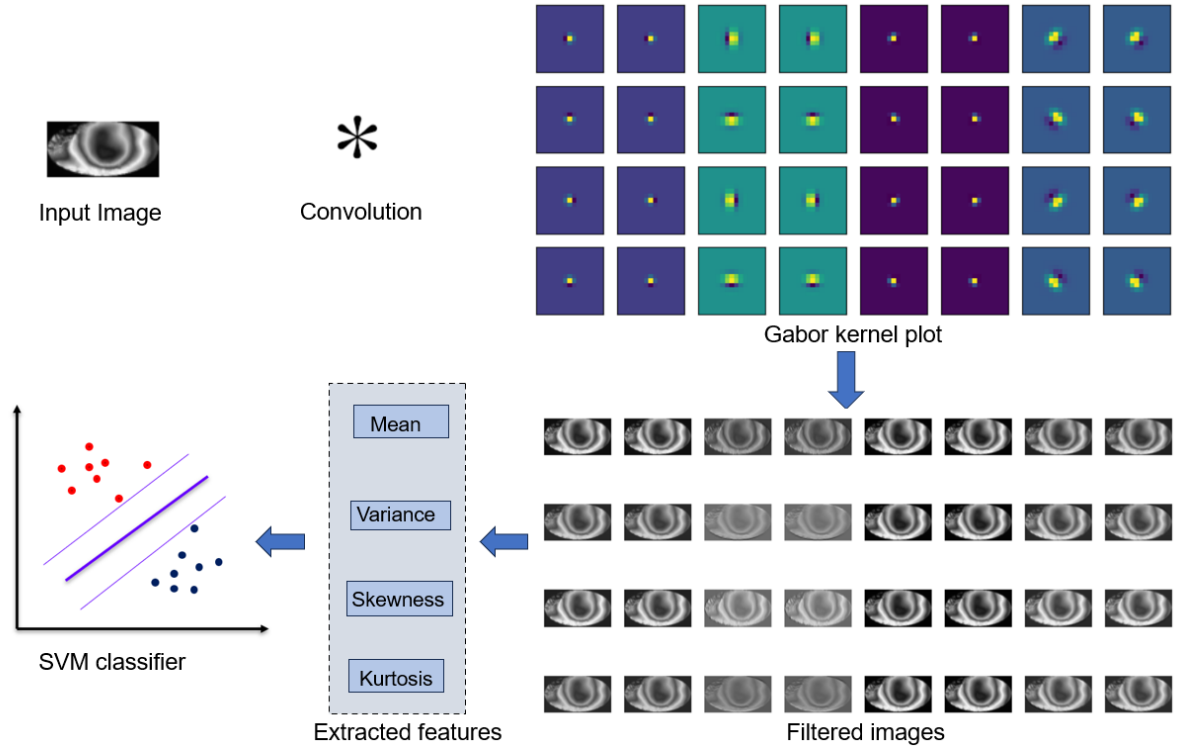

Fig. 8. *Feature extraction using a bank of 32 filters*

Similarly, for a dataset consisting of 800 augmented DR images, this results in a total of 1280 Gabor-filtered output images and for a dataset comprising 850 healthy images, a total of 1024 Gabor-filtered output images are obtained which is fed into SVM.

2.4. Support Vector Machine

SVM is an effective binary classification machine learning technique. SVM excels in finding the optimal decision boundary within the feature space, allowing for the linear separation of two classes in a dataset. In actuality, the majority of data cannot be separated linearly [32]. The kernel functions enable the effective separation of non-linearly separable data. The feature points can be mapped to higher dimensional spaces using the kernel function. In this work, kernel functions with linear, polynomial, radial basis functions and sigmoid have been employed.

SVM in Thermal Image Analysis: When applied to thermal images, SVM offers an invaluable means of extracting meaningful patterns and classifying thermal data effectively. Thermal images often contain intricate temperature variations and subtle nuances that require a powerful classification algorithm. SVMs prove to be well-suited for this task as they can discern intricate thermal features and distinguish between different thermal profiles with a high degree of accuracy [33]. The ability to perform well in high-dimensional feature spaces is especially advantageous in thermal image analysis, where thermal radiation intensity variations must be carefully considered. The SVM classifier's performance has been assessed by considering metrics such as accuracy, sensitivity, and specificity. Additionally, a receiver operating characteristic (ROC) curve has been generated

3. Results and Discussion

The performance of the suggested approach was assessed on an augmented dataset, as detailed in the methodology section. The dataset consists of 800 eye images with a clinical diagnosis of diabetic retinopathy and 850 eye images from control patients who did not exhibit any symptoms of the disease. Statistical methods such as GLCM, SIFT and Gabor parameters were extracted from the IR images of DR and control eyes. The extracted texture features are used as important parameters for SVM classification which are discussed in the following subsections.

3.1. GLCM Features

The GLCM characterizes the input's texture by calculating the number of pixel pair occurrences with a particular value in a specified spatial pattern. The size of the GLCM is dependent on the grey levels of the image. After forming the GLCM, statistical measures were calculated from the matrix. From the normalized GLCM, 4 features are extracted. The extracted features are shown in Table 1.

Table 1. GLCM Features

GLCM FEATURES	NORMAL	ABNORMAL
Energy	0.1001±0.0071	0.108±0.0072
Contrast	26.650±7.8635	28.192±12.1010
Homogeneity	0.5609±0.0685	0.517±0.0938
Correlation	0.9958±0.0020	0.9960±0.0020

The aforementioned texture features are trained by SVM by applying mathematical equations known as the kernel approaches, by mapping the training dataset into a specialized kernel space. Four distinct types of kernel functions—linear, polynomial, radial basis function, and sigmoid—are employed. Particularly, the Radial Basis Function (RBF) kernel proves advantageous for transforming vectors into a high-dimensional feature space when non-linear transformations are needed. Additionally, the RBF kernel improves the overall accuracy, as demonstrated in Table 2.

Table 2. Classification accuracy for GLCM texture feature extraction

SVM Kernel	Accuracy	Sensitivity	Specificity
Linear	58%	43%	7%
Polynomial	54%	14%	87%
Radial Basis Function	**72%**	**73%**	**71%**
Sigmoid	55%	0%	1%

The evaluation of the proposed system's performance is conducted through statistical metrics, including sensitivity and specificity. The receiver operating characteristic (ROC) has been generated. Figure 9 shows the ROC curve for the above four GLCM parameters.

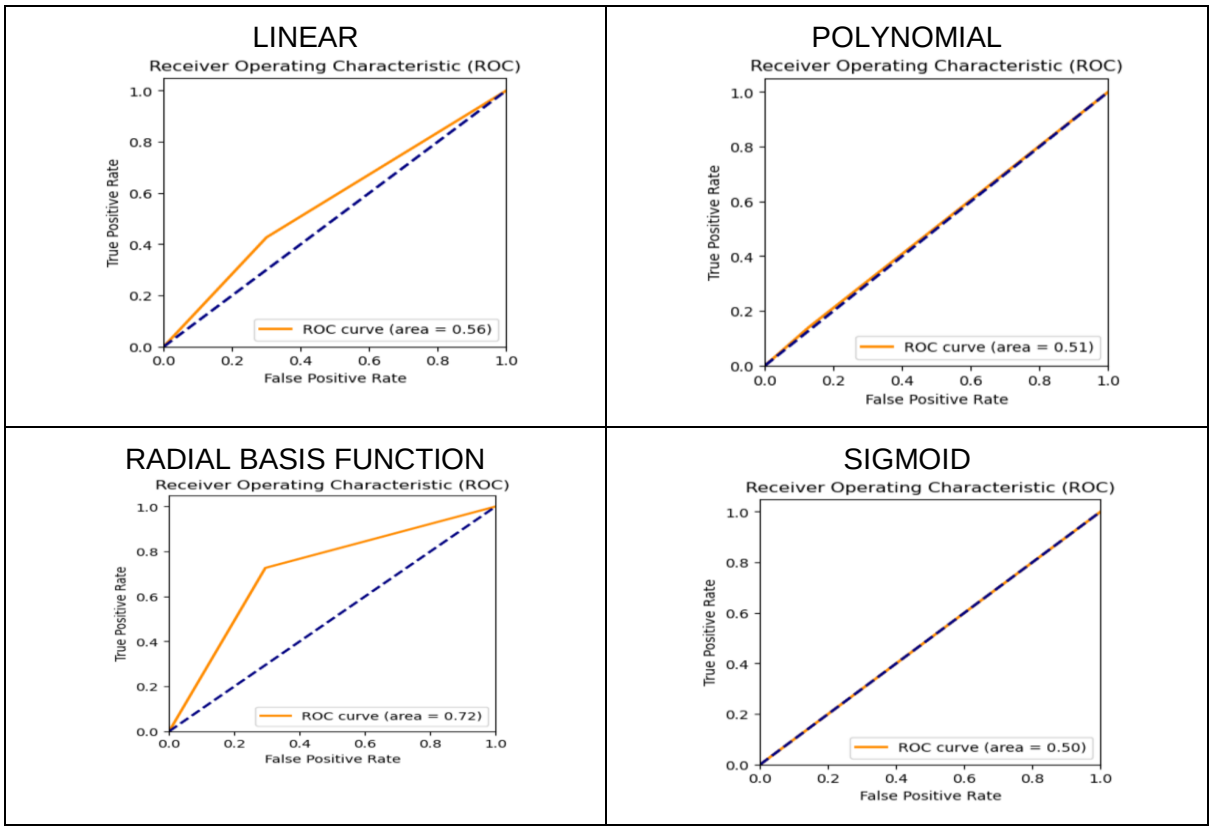

Fig. 9. *ROC analysis of GLCM - SVM kernels*

3.2. SIFT Features

A combination of machine learning and feature extraction techniques to address the critical task of diabetic retinopathy detection. Leveraging the power of Support Vector Machines (SVM) in conjunction with the Scale-Invariant Feature Transform feature extraction method, experiments on a meticulously curated dataset consisting of 850 normal ocular IR images and 800 images affected by diabetic retinopathy was conducted. Initially, scale space selection and keypoints localization is computed as illustrated in Figure 10.

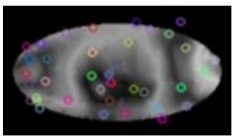

Fig. 10. *Keypoints localization for sample image*

The keypoint descriptor is then created and then normalised to unit length to make it invariant to scale and rotation changes. The Keypoints and Feature descriptors for a sample image is shown below in Figure 11.

```
Number of keypoints detected: 18
Size of the feature descriptors: (18, 128)
```

Fig. 11. *Key Points and Feature descriptors for one image from the sample using OpenCV*

The use of k-means clustering to create a visual lexicon of SIFT descriptors using 100 clusters was one of the essential elements of the methodology that was described. A representative visual word dictionary was made possible by this technique, enabling the accurate characterization and differentiation of image regions according to their distinctive characteristics. In this study, we exploited the simplicity and efficacy of the linear SVM kernel for a simple yet robust

classification strategy for the thermal imaging dataset, finally leading to accurate results. With precision scores of 0.96 and 0.90, as well as recall scores of 0.91 and 0.95, for the "Normal" and "Diseased" classes, respectively, the results highlight the efficacy of this approach. Additionally, F1-scores and overall accuracy of **93%** underscore the robustness of our proposed framework.

3.3. Gabor Transform

Augmented IR images, encompassing both normal and diabetic retinopathy (DR) cases, underwent processing with a Gabor bank, comprising eight distinct orientations, resulting in Gabor filtered output images. Subsequently, texture features were extracted from these images, including measures such as mean, variance, skewness, and kurtosis.as shown in Table 3.

Table 3. Gabor features

GABOR FEATURES	NORMAL	ABNORMAL
Mean	117.25±70.219	91.779±54.955
Variance	10346.37±12258.52	6135.399±7268.255
Skewness	-0.0869±0.0098	-0.03172±0.0152
Kurtosis	-1.5033±0.0362	-1.2877±0.066

These four features are fed into SVM with four kernel functions and the performance of each classifier has been assessed in terms of accuracy, sensitivity and specificity as shown in Table 4. The linear kernel is particularly beneficial when dealing with vectors that can be linearly mapped to a high-dimensional feature space and the kernel increases overall accuracy of 96%, sensitivity of 98% and specificity of 93%. Figure 12 shows the ROC curve for all the four classifiers.

Table 4. Classification accuracy for Gabor texture features

SVM Kernel	Accuracy	Sensitivity	Specificity
Linear	**95.7%**	**98%**	**93%**
Polynomial	71%	68%	70%
Radial Basis Function	77%	55%	1.0%
Sigmoid	60%	55%	67%

The performance analysis of each feature extraction technique is represented in Table 5. In summary, investigation demonstrates that the synergy between GABOR feature extraction and SVM classification yields promising results for the detection of diabetic retinopathy in retinal images. The achieved precision, recall, and overall accuracy rates substantiate the effectiveness of this approach, paving the way for potential advancements in the realm of medical image analysis and automated disease diagnosis. This study underscores the potential of Gabor in conjunction with SVM as a formidable tool in the domain of medical image analysis, offering significant contributions towards enhancing diagnostic accuracy and efficiency.

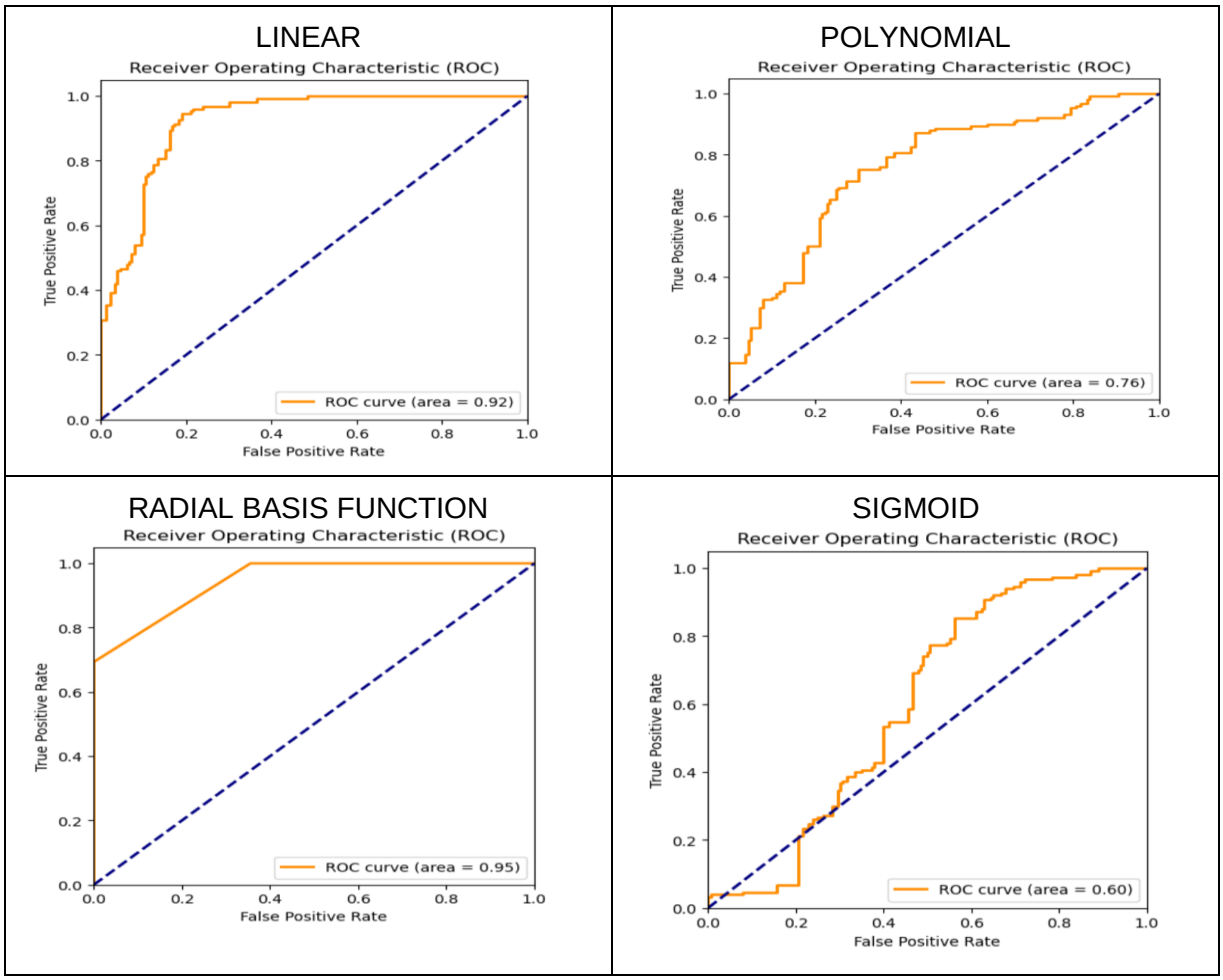

Fig. 12. *ROC analysis of GABOR - SVM kernels*

Table 5. Performance analysis of the feature extraction technique

Feature Extraction technique	Actual Class	Precision	Recall	F1-Score	Support
GLCM	Normal	76%	71%	73%	180
	Abnormal	67%	73%	70%	150
SIFT	Normal	96%	91%	93%	179
	Abnormal	90%	95%	92%	155
Gabor	Normal	99%	93%	96%	180
	Abnormal	92%	99%	96%	150

4. Conclusion

In the proposed work, a non-intrusive procedure has been presented to assess the presence of diabetic retinopathy by analysing real time acquired thermal eye images obtained from 40 DR and 32 control participants. Subsequently, the images undergo pre-processing. Three types of texture features are extracted for this study, specifically GLCM, Gabor features and SIFT features. The classification of diseased and normal eye IR images is done through Support Vector Machine classifier utilizing various kernels with the feature set as input. The simulation results demonstrate that the algorithm is highly efficient in terms of achieving a very high classification accuracy rate for distinguishing diabetic retinopathy from normal eyes. The study compared the classification accuracy of the three types of texture-based features, with the Gabor feature-based classification outperforming the others, achieving an accuracy rate of approximately 95.7%. The results obtained were compared with the other research papers and presented in Table 6.

Table 6. Comparison of results with literature

Related reference	Number of class	Accuracy (%)
A.A. Khan *et al.*, (2018)	2	84.5%
Acharya UH *et al.,* (2015)	2	93.10%
Proposed Model	**2**	**95.7%**

The demonstrated effectiveness of the proposed techniques holds the potential to significantly assist ophthalmologists in more accurate retinal image analysis. This, in turn, could lead to improved early-stage treatment, ultimately contributing to the prevention of blindness. This approach can be further extended to assess different levels of Diabetic Retinopathy. Such a system can be useful in automated large-scale screening.

Acknowledgements

The authors are thankful to Dr. K. Kavithalaksmi for her support. Furthermore, the authors would like to thank the management of Sri Sivasubramaniya Nadar College of Engineering, Kalavakkam, for providing the facilities to carry out this work.

REFERENCES

[1] Shaw JE., Sicree RA., Zimmet PZ., “Global estimates of the prevalence of diabetes for 2010 and 2030”. Diabetes research and clinical practice. 2010 Jan 1;87(1):4-14.

[2] Chen YW., Wu TY., Wong WH., Lee CY., “Diabetic retinopathy detection based on deep convolutional neural networks”. In2018 IEEE international conference on acoustics, speech and signal processing (ICASSP) 2018 Apr 15 (pp. 1030-1034). IEEE.

[3] Zegeye AF., Temachu YZ., Mekonnen CK., “Prevalence and factors associated with Diabetes retinopathy among type 2 diabetic patients at Northwest Amhara Comprehensive Specialized Hospitals, Northwest Ethiopia 202”. BMC ophthalmology. 2023 Jan 5;23(1):9.

[4] Duh EJ., Sun JK., Stitt AW., “Diabetic retinopathy: current understanding, mechanisms, and treatment strategies". JCI insight. 2017 Jul 7;2(14).

[5] Ismael HR., Abdulazeez AM., Hasan DA., “Detection of Diabetic Retinopathy Based on Convolutional Neural Networks: A Review”. Asian Journal of Research in Computer Science. 2021 May 8;8(3):1-5.

[6] Kwasigroch A., Jarzembinski B., Grochowski M., “Deep CNN based decision support system for detection and assessing the stage of diabetic retinopathy”. In2018 International Interdisciplinary PhD Workshop (IIPhDW) 2018 May 9 (pp. 111-116). IEEE.

[7] Naidorf-Rosenblatt H., Landau-Part D., Moisseiev J., Alhalel A., Huna-Baron R., Skaat A., Pilus S., Levi L, Leshno A., “Ocular surface temperature differences in retinal vascular diseases”. Retina. 2022 Jan 1;42(1):152-8.

[8] Sodi A., Giambene B., Miranda P., Falaschi G., Corvi A., Menchini U., “Ocular surface temperature in diabetic retinopathy: a pilot study by infrared thermography”. European journal of Ophthalmology. 2009 Nov;19(6):1004-8.

[9] Land MR., Patel PA., Bui T., Jiao C., Ali A., Ibnamasud S., Patel PN., Sheth V., “Examining the Role of Telemedicine in Diabetic Retinopathy.” Journal of Clinical Medicine. 2023 May 18;12(10):3537.

[10] Perpetuini D., Filippini C., Cardone D., Merla A., “An overview of thermal infrared imaging-based screenings during pandemic emergencies”. International Journal of Environmental Research and Public Health. 2021 Mar 22;18(6):3286.

[11] Tan JH., Ng EY., Acharya UR., Chee C., “Infrared thermography on ocular surface temperature: a review”. Infrared physics & technology. 2009 Jul 1;52(4):97-108.

[12] Lin JW., Lu MH., Lin YH., “A thermal camera based continuous body temperature measurement system”. InProceedings of the IEEE/CVF International Conference on Computer Vision Workshops 2019 (pp. 0-0).

[13] Padmapriya N., Venkateswaran N., Kannan T., Madhuri MS., “Assessment of Glaucoma with ocular thermal images using GLCM techniques”. In12th International Conference on Quantitative Infrared Thermography, Mamallapuram, India 2015.

[14] Raut R., Sapkal A., Ingale V., Borkar P., Bhanarkar P., “Assessment of diabetic retinopathy progression using CNN from ocular thermal images”. Soft Computing. 2023 Apr 26:1-7.

[15] Chandrasekar B., Rao AP., Murugesan M., Subramanian S., Sharath D., Manoharan U., Prodip B., Balasubramaniam V., “Ocular surface temperature measurement in diabetic retinopathy”. Experimental Eye Research. 2021 Oct 1;211:108749.

[16] Selvarasu N., Nachiappan A., Nandhitha NM., “Euclidean distance based color image segmentation of abnormality detection from pseudo color thermographs”. International Journal of Computer Theory and Engineering. 2010 Aug 1;2(4):514.

[17] Purslow C., Wolffsohn J. “The relation between physical properties of the anterior eye and ocular surface temperature”. Optometry and Vision Science. 2007 Mar 1;84(3):197-201.

[18] Lin X., Ma YL, Ma LZ., Zhang RL., “A survey for image resizing”. Journal of Zhejiang University SCIENCE C. 2014 Sep;15(9):697-716.

[19] Abdollahi B., Tomita N., Hassanpour S., “Data augmentation in training deep learning models for medical image analysis”. Deep learners and deep learner descriptors for medical applications. 2020:167-80.

[20] Mikołajczyk A., Grochowski M., “Data augmentation for improving deep learning in image classification problem”. In2018 international interdisciplinary PhD workshop (IIPhDW) 2018 May 9 (pp. 117-122). IEEE.

[21] Mohanaiah P., Sathyanarayana P., GuruKumar L., “Image texture feature extraction using GLCM approach”. International journal of scientific and research publications. 2013 May;3(5):1-5.

[22] Wiecek B., Danych R., Zwolenik Z., Jung A., Zuber J., “Advanced thermal image processing for medical and biological applications”. In2001 Conference Proceedings of the 23rd Annual International Conference of the IEEE Engineering in Medicine and Biology Society 2001 Oct 25 (Vol. 3, pp. 2805-2807). IEEE.

[23] Usha R., Perumal K., “SVM classification of brain images from MRI scans using morphological transformation and GLCM texture features”. International journal of computational systems engineering. 2019;5(1):18-23.

[24] Li D., Gong J., Li D., “SIFT Based Feature Matching Algorithm for Cartoon Plagiarism Detection”. InNew Approaches for Multidimensional Signal Processing: Proceedings of International Workshop, NAMSP 2021 2022 Mar 22 (pp. 79-87). Singapore: Springer Singapore.

[25] Cui S., Jiang H., Wang Z., Shen C., “Application of neural network based on SIFT local feature extraction in medical image classification”. In2017 2nd International Conference on Image, Vision and Computing (ICIVC) 2017 Jun 2 (pp. 92-97). IEEE.

[26] Christlein V., Gropp M., Fiel S., Maier A., “Unsupervised feature learning for writer identification and writer retrieval”. In2017 14th IAPR International Conference on Document Analysis and Recognition (ICDAR) 2017 Nov 9 (Vol. 1, pp. 991-997). IEEE.

[27] Khan S., Hussain M., Aboalsamh H., Bebis G., “A comparison of different Gabor feature extraction approaches for mass classification in mammography”. Multimedia Tools and Applications. 2017 Jan;76:33-57.

[28] SwagotaBera D., Sharma M., Singh B., “Feature extraction and analysis using Gabor filter and higher order statistics for the JPEG steganography”. Int. J. Appl. Eng. Res. 2018;13:2945-54.

[29] Kamarainen JK., “Gabor features in image analysis”. In2012 3rd international conference on image processing theory, tools and applications (IPTA) 2012 Oct 15 (pp. 13-14). IEEE.

[30] Wang X., Ding X., Liu C., “Gabor filters-based feature extraction for character recognition. Pattern recognition”. 2005 Mar 1;38(3):369-79.

[31] Khan AA., Arora AS., “Breast cancer detection through gabor filter based texture features using thermograms images”. In2018 First international conference on secure cyber computing and communication (ICSCCC) 2018 Dec 15 (pp. 412-417). IEEE.

[32] Acharya UR., Ng EY., Eugene LW., Noronha KP., Min LC., Nayak KP., Bhandary SV., “Decision support system for the glaucoma using Gabor transformation”. Biomedical Signal Processing and Control. 2015 Jan 1;15:18-26.

[33] Vardasca R., Vaz L., Mendes J., “Classification and decision making of medical infrared thermal images”. Classification in BioApps: Automation of Decision Making. 2018:79-104.